Structural Engineering and Mechanics, Vol. 14, No. 1 (2002) 99-118
DOI: http://dx.doi.org/10.12989/sem.2002.14.1.099

Semi-analytical elastostatic analysis of two-dimensional domains with similar boundaries

Andrew J. Deeks†

Department of Civil and Resource Engineering, The University of Western Australia, Crawley, Western Australia 6009, Australia

(Received December 20, 2001, Accepted April 16, 2002)

Abstract. The scaled-boundary finite element method is a novel semi-analytical technique, combining the advantages of the finite element and the boundary element methods with unique properties of its own. The method works by weakening the governing differential equations in one coordinate direction through the introduction of shape functions, then solving the weakened equations analytically in the other (radial) coordinate direction. These coordinate directions are defined by the geometry of the domain and a scaling centre. This paper presents a general development of the scaled boundary finite-element method for two-dimensional problems where two boundaries of the solution domain are similar. Unlike three-dimensional and axisymmetric problems of the same type, the use of logarithmic solutions of the weakened differential equations is found to be necessary. The accuracy and efficiency of the procedure is demonstrated through two examples. The first of these examples uses the standard finite element method to provide a comparable solution, while the second combines both solution techniques in a single analysis. One significant application of the new technique is the generation of transition super-elements requiring few degrees of freedom that can connect two regions of vastly different levels of discretisation.

Key words: scaled boundary finite-element method; similarity; plane stress; plane strain; axisymmetry; transition element.

1. Introduction

Elastostatic analysis has been dominated by the finite element method (Zienkiewicz and Taylor 1989, Szabó and Babuška 1991) and to a lesser extent by the boundary element method (Brebbia and Walker 1980, Banerjee and Butterfield 1981) for over four decades. Despite this, alternative methods such as the finite strip method (Cheung 1976, Cheung, Li and Chidiac 1996) are of practical interest and are computationally more efficient than the conventional methods for domains of particular restricted geometry. This paper addresses another alternative method that exhibits qualitative and quantitative advantages over the conventional finite element and boundary element methods for particular classes of problems. Here the method is applied to domains with two geometrically similar boundaries. The new method may be combined with the conventional finite element method, providing super-elements that can connect regions of vastly different levels of discretisation.

† Senior Lecturer

The scaled boundary finite-element method is a novel semi-analytical approach to continuum analysis developed by Wolf and Song. The method was originally derived to compute the dynamic stiffness of an unbounded domain (Song and Wolf 1996), and was based on a 'cloning' technique in which the analytical limit is taken as the width of the cloned finite-element cell tends to zero. The method proved to be more general than initially envisaged, with later developments allowing analysis of incompressible material and bounded domains (Wolf and Song 1996), and the inclusion of body loads (Song and Wolf 1999). The complexity of the original derivation of the technique led to the development of a weighted residual formulation (Song and Wolf 1997, Wolf and Song 2001), and recently a simplified virtual work derivation for elastostatics (Deeks and Wolf 2002a & 2002b).

The scaled boundary finite-element method works by weakening the governing differential equations in one (circumferential) coordinate direction s through the introduction of shape functions, then solving the weakened equations analytically in the other (radial) coordinate direction ξ. These coordinate directions are defined by the geometry of the domain and a scaling centre. In most previous work unbounded domains not containing the scaling centre (Fig. 1a) and bounded domains containing the scaling centre (Fig. 1b) have been treated. Domains which are bounded on two sides by lines radiating from the scaling centre (Figs. 1c and 1d) have also been addressed. Boundaries

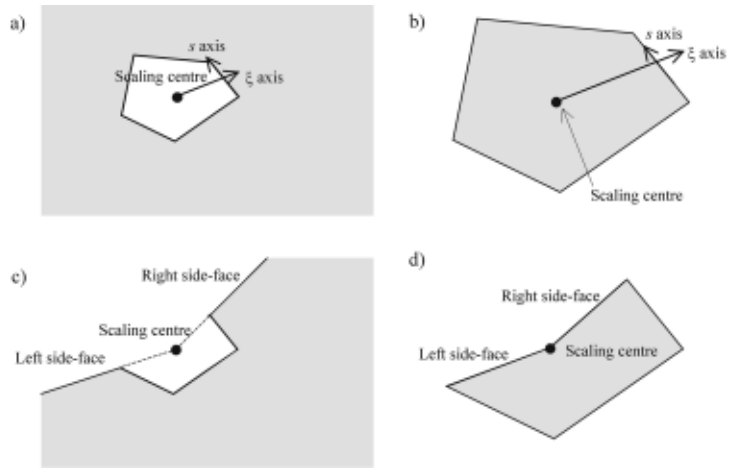

Fig. 1 Types of domains addressed in previous work

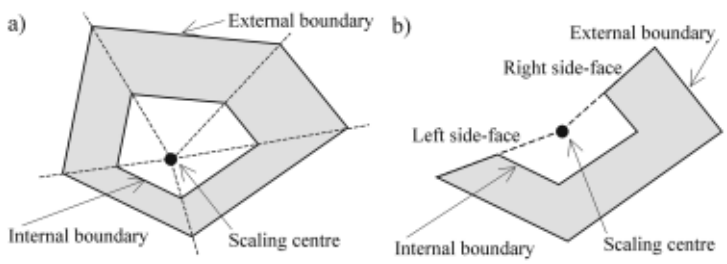

Fig. 2 Domains treated in this work-a) without side-faces, b) with side-faces

falling on such radial lines are termed side-faces.

The dynamic stiffness of domains with two similar boundaries has been derived by Song and Wolf (1998) using the scaled boundary finite-element method. However, this derivation is restricted to three-dimensional and axisymmetric problems.

This paper presents a general development of the scaled boundary finite-element method for two-dimensional elastostatic problems where two boundaries of a domain are similar (Figs. 2a and 2b). The equations are developed for two-dimensional problems of plane stress and plane strain. The virtual work derivation presented by Deeks and Wolf (2002a) is extended to the problem with two similar boundaries. The two similar boundaries are termed internal and external boundaries, as indicated in Fig. 2. Unbounded domains occur when the external boundary is positioned at infinity, while bounded domains containing the scaling centre are generated when the internal boundary is placed at the scaling centre.

2. Scaled boundary finite-element method derivation

In the absence of body loads, with the internal stresses designated as $\{\sigma(x, y)\}$, enforcing internal equilibrium leads to the differential equation

$$[L]^T \{\sigma(x, y)\} = \{0\} \tag{1}$$

which must be satisfied at every point within the domain ("volume" V). $[L]$ is the linear operator relating the strains $\{\varepsilon(x, y)\}$ and the displacements $\{u(x, y)\}$

$$\{\varepsilon(x, y)\} = [L]\{u(x, y)\} \tag{2}$$

The stresses and strains are related by the elasticity matrix $[D]$

$$\{\sigma(x, y)\} = [D]\{\varepsilon(x, y)\} \tag{3}$$

Definitions of the vector components, the linear operator and the elasticity matrices for problems of plane stress and plane strain are given in Appendix A.

The domain is bounded by an external boundary, which is denoted by S_e, and an internal boundary, denoted by S_i. If S_e and S_i are similar, each point on S_e corresponds to a point on S_i, and all lines passing through pairs of such point intersect at a single point (as illustrated in Fig. 2a). This point is designated (x_0, y_0), and will be referred to as the scaling centre. The internal and external boundaries may be treated as scaled versions of a single curve, S, which, together with the scaling centre, defines the geometry of the domain. If the curve S is not closed, the boundary of the domain also contains two distinct side-faces, as illustrated in Fig. 2b, otherwise the internal and external boundaries are disjoint, as indicated in Fig. 2a. In such cases the domain can be considered to contain two coincident side-faces across which equilibrium and compatibility are maintained.

The curve S can be represented by a set of points $(x_0 + x_s(s), y_0 + y_s(s))$, where s is a coordinate measuring the distance around the curve from a selected origin. Introducing a normalised radial coordinate ξ which is chosen to have unit value on S, the external boundary is defined by $\xi = \xi_e$ while the internal boundary is defined by $\xi = \xi_i$. Any point (x, y) within the domain can be identified in terms of s and ξ, which are referred to as the scaled boundary coordinates. The scaled boundary and Cartesian coordinate systems are related by the scaling equations

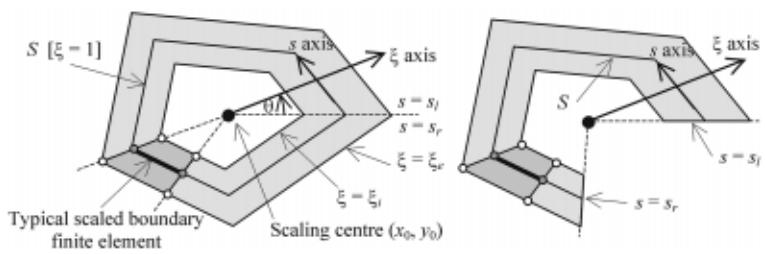

Fig. 3 Scaled boundary coordinate definition: left, with a closed defining curve; right, with an open defining curve

$$x = x_0 + \xi x_s(s) \tag{4a}$$

$$y = y_0 + \xi y_s(s) \tag{4b}$$

Domains defined with open and closed curves are shown in Fig. 3, along with the scaled boundary coordinate systems. The solution domain V in each case is the region defined by $\xi_i \le \xi \le \xi_e$ and $s_l \le s \le s_r$. A limitation on the geometry of the domains is that the derivative of the circumferential angle θ with respect to s remains positive over the entire curve S.

In the development which follows, displacement and stress components are retained in the original Cartesian coordinate directions, while position is specified in terms of the scaled boundary coordinates. Boundary conditions are specified at all boundary points on either displacements or surface tractions.

The scaled boundary finite-element method seeks an approximate solution for the displacement field $\{u(\xi, s)\}$ in the form

$$\{u_h(\xi, s)\} = \sum_{i=1}^{n} N_i(s) u_{hi}(\xi) = [N(s)]\ \{u_h(\xi)\} \tag{5}$$

The subscript h is used to indicate approximate quantities that are determined in the course of the analysis and depend on the n predefined shape functions $N_i(s)$ selected to represent the variation of the displacement field in the s direction. Conventionally the curve S is broken into two- or three-noded isoparametric line elements, and polynomial shape functions defined over each element in the standard finite element manner. Each line element then represents an elemental 'volume' of the domain, bounded by two radial node lines and the boundaries S_i and S_e. Fig. 3 illustrates a typical two-noded scaled boundary finite element and the region of the domain modelled by this element. The shape functions interpolate in the circumferential direction between analytical functions that describe the variation of the displacement along radial lines passing through each node point on S (the node lines). The vector $\{u_h(\xi)\}$ is therefore a set of n functions analytical in ξ. Each node point on the curve S scales to a node on the external boundary and a node on the internal boundary. The displacements at the external boundary nodes are $\{u_h(\xi_e)\}$, while the displacements at the internal boundary nodes are $\{u_h(\xi_i)\}$.

Mapping the linear operator to the scaled boundary coordinate system using standard methods (see Appendix B)

$$[L] = [L^1]\frac{\partial}{\partial x} + [L^2]\frac{\partial}{\partial y} = [b^1(s)]\frac{\partial}{\partial \xi} + \frac{1}{\xi}[b^2(s)]\frac{\partial}{\partial s} \tag{6}$$

where $[b^1(s)]$ and $[b^2(s)]$ are dependent only on the definition of the curve S (see Eqs. (B9) and (B10)).

Combining Eqs. (2) and (3) and substituting Eq. (6), the approximate stresses are

$$\{\sigma_h(\xi, s)\} = [D]\ \{\varepsilon_h(\xi, s)\} = [D]\ [B^1(s)]\ \{u_h(\xi)\},_\xi + \frac{1}{\xi}[D]\ [B^2(s)]\{u_h(\xi)\} \tag{7}$$

where, for convenience

$$[B^1(s)] = [b^1(s)][N(s)] \tag{8}$$

$$[B^2(s)] = [b^2(s)][N(s)],_s \tag{9}$$

An alternative formulation of the equilibrium requirement is the virtual work statement. Using $\{\delta u(x, y)\}$ to represent a virtual displacement field, and

$$\{\delta\varepsilon(\xi, s)\} = [L]\{\delta u(\xi, s)\} \tag{10}$$

to represent the corresponding virtual strains, and designating the distance around the external boundary as s_e and the distance around the internal boundary as s_i, the virtual work equation states that

$$\int_V \{\delta\varepsilon(\xi, s)\}^T\{\sigma(\xi, s)\}\ dV - \int_{S_i}\{\delta u(\xi_i, s)\}^T\{t(\xi_i, s)\}\ ds_i - \int_{S_e}\{\delta u(\xi_e, s)\}^T\{t(\xi_e, s)\}\ ds_e$$
$$- \int_{\xi_i}^{\xi_e}\{\delta u(\xi, s_l)\}^T\{t(\xi, s_l)\}\ |J(s_l)|d\xi - \int_{\xi_i}^{\xi_e}\{\delta u(\xi, s_r)\}^T\{t(\xi, s_r)\}\ |J(s_r)|\ d\xi = 0 \tag{11}$$

The first term in this equation is the internal virtual work. The remaining terms represent the external virtual work done by the tractions acting on the boundaries. The second term results from the tractions on the internal boundary, $\{t(\xi_i, s)\}$, the third term from tractions $\{t(\xi_e, s)\}$ on the external boundary, the fourth term from the tractions $\{t(\xi, s_l)\}$ on the left side face and the final term from the tractions $\{t(\xi, s_r)\}$ on the right side-face. If the defining curve of the domain is closed, $\{t(\xi, s_l)\} = -\{t(\xi, s_l)\}$, and the last two terms cancel. If the defining curve is open, but there are no tractions on the side-faces, the last two terms are both zero.

When Eq. (11) is satisfied for all virtual displacement fields, equilibrium is satisfied in the strong sense. If it is satisfied for a subset of virtual displacement fields, equilibrium is only satisfied in a weak sense.

A virtual displacement field is formed using the shape functions $[N(s)]$ to interpolate between the radial node lines in the circumferential direction (the Galerkin approach). This virtual displacement field is of the form (analogous to Eq. (5))

$$\{\delta u(\xi, s)\} = [N(s)]\{\delta u(\xi)\} \tag{12}$$

where $\{\delta u(\xi)\}$ contains n functions describing the variation of the virtual displacements in the radial direction. $\{\delta u(\xi_e)\}$ contains the virtual nodal displacements on the external boundary, while

$\{\delta u(\xi_i)\}$ contains the virtual nodal displacements on the external boundary. The corresponding virtual strain field is of the form (analogous to Eq. (7))

$$\{\delta\varepsilon(\xi, s)\} = [B^1(s)]\,\{\delta u(\xi)\}_{,\xi} + \frac{1}{\xi}[B^2(s)]\,\{\delta u(\xi)\} \tag{13}$$

Eq. (B6) indicates that

$$dV = |J(s)|\,\xi\, d\xi\, ds \tag{14}$$

where $|J(s)|$ is the Jacobian evaluated at the curve S (i.e., at $\xi = 1$).

Substituting Eqs. (7), (13) and (14), integrating the area integrals containing $\{\delta u(\xi)\}_{,\xi}$ by parts with respect to ξ using Green's Theorem, introducing line integrals evaluated around the boundaries, the internal virtual work term is expanded to

$$\begin{aligned}
\int_V \{\delta\varepsilon(\xi, s)\}^T\{\sigma_h(\xi, s)\}dV \;=\; & \int_S \{\delta u(\xi)\}^T[B^1(s)]^T[D][B^1(s)]\xi\{u_h(\xi)\}_{,\xi}\,|J(s)|\,ds\Big|_{\xi=\xi_i}^{\xi=\xi_e} \\
& -\int_S\int_{\xi_i}^{\xi_e}\{\delta u(\xi)\}^T[B^1(s)]^T[D][B^1(s)]\{\{u_h(\xi)\}_{,\xi} + \xi\{u_h(\xi)\}_{,\xi\xi}\}\,|J(s)|d\xi\, ds \\
& + \int_S\{\delta u(\xi)\}^T[B^1(s)]^T[D][B^2(s)]\{u_h(\xi)\}\,|J(s)|\,ds\Big|_{\xi=\xi_i}^{\xi=\xi_e} \\
& -\int_S\int_{\xi_i}^{\xi_e}\{\delta u(\xi)\}^T[B^1(s)]^T[D][B^2(s)]\{u_h(\xi)\}_{,\xi}\,|J(s)|\,d\xi\, ds \\
& + \int_S\int_{\xi_i}^{\xi_e}\{\delta u(\xi)\}^T[B^2(s)]^T[D][B^1(s)]\{u_h(\xi)\}_{,\xi}\,|J(s)|\,d\xi\, ds \\
& + \int_S\int_{\xi_i}^{\xi_e}\{\delta u(\xi)\}^T[B^2(s)]^T[D][B^2(s)]\frac{1}{\xi}\{u_h(\xi)\}\,|J(s)|\,d\xi\, ds
\end{aligned} \tag{15}$$

For convenience the following coefficient matrices are introduced:

$$[E^0] = \int_S [B^1(s)]^T[D][B^1(s)]\,|J(s)|\,ds \tag{16a}$$

$$[E^1] = \int_S [B^2(s)]^T[D][B^1(s)]\,|J(s)|\,ds \tag{16b}$$

$$[E^2] = \int_S [B^2(s)]^T[D][B^2(s)]\,|J(s)|\,ds \tag{16c}$$

These integrals can be computed element by element over S, and assembled together for the entire curve. Eq. (15) is then expressed as

$$\int_V \{\delta\varepsilon(\xi, s)\}^T\{\sigma_h(\xi, s)\}\ dV = \{\delta u(\xi_e)\}^T\{\xi_e[E^0]\{u_h(\xi_e)\},_\xi + [E^1]^T\{u_h(\xi_e)\}\}$$
$$-\{\delta u(\xi_i)\}^T\{\xi_i[E^0]\{u_h(\xi_i)\},_\xi + [E^1]^T\{u_h(\xi_i)\}\}$$
$$-\int_{\xi_i}^{\xi_e}\{\delta u(\xi)\}^T\left\{[E^0]\xi\{u_h(\xi)\},_{\xi\xi} + [[E^0] + [E^1]^T - [E^1]]\{u_h(\xi)\},_\xi - [E^2]\frac{1}{\xi}\{u_h(\xi)\}\right\} d\xi \quad (17)$$

On substitution of Eq. (12), and noting that the distance around the external boundary $s_e = \xi_e\, s$ and the distance around the internal boundary $s_i = \xi_i\, s$, the external virtual work term for the external boundary in Eq. (11) becomes

$$\int_{S_e}\{\delta u(\xi_e, s)\}^T\{t(\xi_e, s)\}\ ds_e = \{\delta u(\xi_e)\}^T\int_S[N(s)]^T\{t(\xi_e, s)\}\ \xi_e\ ds = \{\delta u(\xi_e)\}^T\{P_e\} \quad (18)$$

where $\{P_e\}$ are the equivalent nodal forces due to the boundary tractions acting on the external boundary determined in the conventional finite element manner as

$$\{P_e\} = \int_S[N(s)]^T\{t(\xi_e, s)\}\ \xi_e\ ds \quad (19)$$

and the external virtual work term for the internal boundary becomes

$$\int_{S_i}\{\delta u(\xi_i, s)\}^T\{t(\xi_i, s)\}\ ds_i = \{\delta u(\xi_i)\}^T\int_S[N(s)]^T\{t(\xi_i, s)\}\ \xi_i\ ds = \{\delta u(\xi_i)\}^T\{P_i\} \quad (20)$$

where $\{P_i\}$ are the conventional equivalent nodal forces due to the boundary tractions acting on the internal boundary

$$\{P_i\} = \int_S[N(s)]^T\{t(\xi_i, s)\}\ \xi_i\ ds \quad (21)$$

On substitution of Eq. (12) the external virtual work terms for the side-faces may be combined as

$$\int_{\xi_i}^{\xi_e}\{\delta u(\xi)\}\{F_t(\xi)\}\ d\xi \quad (22)$$

where

$$\{F_t(\xi)\} = [N(s_l)]^T\{t(\xi, s_l)\}\ |J(s_l)| + [N(s_r)]^T\{t(\xi, s_r)\}\ |J(s_r)| \quad (23)$$

The complete virtual work equation becomes

$$\{\delta u(\xi_e)\}^T\{\xi_e[E^0]\{u_h(\xi_e)\},_\xi + [E^1]^T\{u_h(\xi_e)\}\} - \{\delta u(\xi_e)\}^T\{P_e\}$$
$$-\{\delta u(\xi_i)\}^T\{\xi_i[E^0]\{u_h(\xi_i)\},_\xi + [E^1]^T\{u_h(\xi_i)\}\} - \{\delta u(\xi_i)\}^T\{P_i\}$$
$$-\int_{\xi_i}^{\xi_e}\{\delta u(\xi)\}^T\left\{[E^0]\xi\{u_h(\xi)\},_{\xi\xi} + [[E^0] + [E^1]^T - [E^1]]\{u_h(\xi)\},_\xi - [E^2]\frac{1}{\xi}\{u_h(\xi)\} + \{F_t(\xi)\}\right\} d\xi = \{0\} \quad (24)$$

In order for Eq. (24) to be satisfied for all $\{\delta u(\xi)\}$ the following conditions must be satisfied:

$$\{P_e\} = \xi_e[E^0]\{u_h(\xi_e)\}_{,\xi} + [E^1]^T\{u_h(\xi_e)\} \tag{25}$$

$$\{P_i\} = -\xi_i[E^0]\{u_h(\xi_i)\}_{,\xi} - [E^1]^T\{u_h(\xi_i)\} \tag{26}$$

$$[E^0]\xi^2\{u_h(\xi)\}_{,\xi\xi} + [[E^0] + [E^1]^T - [E^1]]\xi\{u_h(\xi)\}_{,\xi} - [E^2]\{u_h(\xi)\} + \xi\{F_t(\xi)\} = \{0\} \tag{27}$$

Eqs. (25)-(27) is a collection of $n \times n$ equations of similar type, whose solution is given in the next section. Eq. (27) is the scaled boundary finite-element equation in displacement, which is independent of the radial extent of the domain. Eqs. (25) and (26) enforce the boundary conditions at the external and internal boundaries respectively. For bounded domains containing the scaling centre the internal boundary is located at the scaling centre ($\xi_i = 0$) and the curve S may be placed at the external boundary ($\xi_e = 1$). For unbounded domains the external boundary is located at infinity ($\xi_e = \infty$) and S may be placed at the internal boundary ($\xi_i = 1$). These cases have been treated in most previous work. Although it is often convenient to place S at one of the boundaries, it is not essential, and the technique described here will give the same results irrespective of the positioning of S.

3. Solution procedure

When there is no contribution from side-face loads (the defining curve is closed or the side-face tractions are zero) Eq. (27) becomes a homogeneous set of Euler-Cauchy differential equations, the solution of which may be found in the form

$$\{u_h(\xi)\} = c_1\xi^{-\lambda_1}\{\phi_1\} + c_2\xi^{-\lambda_2}\{\phi_2\} + \ldots \tag{28}$$

where the exponents $-\lambda_i$ and corresponding vectors $\{\phi_i\}$ may be interpreted as independent modes of deformation which closely satisfy internal equilibrium in the ξ direction. (The negative sign is adopted for consistency with earlier work (Wolf and Song 1996), in which the method is derived for unbounded domains.) The integration constants c_i represent the contribution of each mode to the solution, and are dependent on the boundary conditions.

The displacements for each mode take the form (omitting the subscript)

$$\{u(\xi)\} = \xi^{-\lambda}\{\phi\} \tag{29}$$

The vector $\{\phi\}$ can be identified as the modal displacements at the node points on curve S, while λ can be identified as a modal scaling factor for the 'radial' direction. The displacements at the internal and external boundary nodes are determined by scaling the displacements at the node points as

$$\{\phi_i\} = \xi_i^{-\lambda}\{\phi\} \tag{30}$$

and

$$\{\phi_e\} = \xi_e^{-\lambda}\{\phi\} \tag{31}$$

respectively.

Substituting Eq. (29) into Eq. (27) yields the quadratic eigenproblem

$$[\lambda^2[E^0] - \lambda[[E^1]^T - [E^1]] - [E^2]]\{\phi\} = \{0\} \tag{32}$$

Solution of this eigenproblem yields $2n$ modes. The eigenvectors contain n modal displacements $\{\phi\}$. Any particular solution is a linear combination of these modes. The modal displacements at all boundary nodes are obtained by applying Eqs. (30) and (31), generating $2n$ displacements for each mode. The equivalent nodal forces required at the boundaries to equilibrate each displacement mode are obtained by substituting Eq. (29) into Eqs. (25) and (26) as

$$\{q_i\} = -\xi_i^{-\lambda}[[E^1]^T - \lambda[E^0]]\{\phi\} \tag{33}$$

and

$$\{q_e\} = \xi_e^{-\lambda}[[E^1]^T - \lambda[E^0]]\{\phi\} \tag{34}$$

In two-dimensional situations where neither side-face is restrained, two orthogonal rigid body translation modes appear twice on solution of the quadratic eigenproblem. If restraint is applied to either side-face in one direction, the rigid body translation mode in the unrestrained direction appears twice. Using d to represent the number of directions in which restraint is provided to a side-face (0, 1 or 2), and letting $r = 2 - d$, the number of independent displacement modes is $2n - r$. However, a total of $2n$ independent modes is required to allow the stiffness matrix relative to the $2n$ boundary degrees of freedom to be generated. The additional r modes can be found in the form

$$\{u(\xi)\} = \{\psi_{ln}\} \ln \xi + \{\phi_{ln}\} \tag{35}$$

The coefficient matrices $\{\psi_{ln}\}$ and $\{\phi_{ln}\}$ are constructed to ensure Eq. (35) satisfies Eq. (27). Full details of this procedure are described by Deeks and Wolf (2002c), who determine the stiffness of an unbounded two-dimensional domain. The displacements at the internal and external boundary nodes are determined as

$$\{\phi_i\} = \{\psi_{ln}\} \ln \xi_i + \{\phi_{ln}\} \tag{36}$$

and

$$\{\phi_e\} = \{\psi_{ln}\} \ln \xi_e + \{\phi_{ln}\} \tag{37}$$

respectively. Corresponding nodal forces at the internal and external boundaries are determined as

$$\{q_i\} = -[E^0]\{\psi_{ln}\} - [E^1]^T\{\phi_{ln}\} \tag{38}$$

and

$$\{q_e\} = [E^0]\{\psi_{ln}\} + [E^1]^T\{\phi_{ln}\} \tag{39}$$

A matrix $[\Phi]$ with $2n$ rows and $2n$ columns is constructed by placing the boundary node displacements for the $2n - r$ independent modes and the r logarithmic modes in the columns, where each column corresponds to one mode. A corresponding square nodal force matrix $[Q]$ of dimension $2n$ is constructed by placing the boundary nodal forces for each mode in the columns.

For any set of boundary node displacements $\begin{Bmatrix} \{u_h(\xi_i)\} \\ \{u_h(\xi_e)\} \end{Bmatrix}$ the integration constants required to satisfy Eq. (28) at both $\xi = \xi_i$ and $\xi = \xi_e$ are

$$\{c\} = [\Phi]^{-1} \begin{Bmatrix} \{u_h(\xi_i)\} \\ \{u_h(\xi_e)\} \end{Bmatrix} \tag{40}$$

The equivalent nodal forces required to cause these displacements are

$$\begin{Bmatrix} \{P_i\} \\ \{P_e\} \end{Bmatrix} = [Q]\{c\} = [Q][\Phi]^{-1} \begin{Bmatrix} \{u_h(\xi_i)\} \\ \{u_h(\xi_e)\} \end{Bmatrix} \tag{41}$$

The stiffness matrix of the domain is therefore

$$[K] = [Q]\,[\Phi]^{-1} \tag{42}$$

and the equilibrium requirement becomes

$$[K] \begin{Bmatrix} \{u_h(\xi_i)\} \\ \{u_h(\xi_e)\} \end{Bmatrix} - \begin{Bmatrix} \{P_i\} \\ \{P_e\} \end{Bmatrix} = \begin{Bmatrix} 0 \\ 0 \end{Bmatrix} \tag{43}$$

Boundary conditions place constraints on subsets of the boundary nodal displacements and equivalent nodal forces, and the solution proceeds in the same manner as in standard finite element analysis.

The integration constants are then obtained using Eq. (40), and the displacement field recovered as

$$\{u_h(\xi, s)\} = [N(s)] \sum_{i=1}^{2n-r} c_i \xi^{-\lambda_i} \{\phi_i\} + \sum_{i=1}^{r} \{c_{2n-i}\{\psi_{ln\,i}\} \ln \xi + \{\phi_{ln\,i}\}\} \tag{44}$$

The stress field is obtained by substituting Eq. (44) into (7) as

$$\{\sigma_h(\xi, s)\} = [D] \left\{ \sum_{i=1}^{2n-r} c_i \xi^{-\lambda_i - 1} [-\lambda_i [B^1(s)] + [B^2(s)]] \{\phi_i\} \right.$$
$$\left. + \sum_{i=1}^{r} c_{2n-i} \xi^{-1} \{[B^2(s)]\{\phi_{ln\,i}\} + [B^1(s)]\{\psi_{ln\,i}\}\} \right\} \tag{45}$$

If the domain is unbounded ($\xi_e = \infty$), the boundary condition on the displacement at the external boundary is zero. This determines n of the integration constants $\{c\}$, and only the remaining n modes are used to construct the stiffness matrix (which is now of dimension n and includes only the nodal degrees of freedom on the internal boundary). Similarly, if the domain is bounded and contains the scaling centre ($\xi_i = 0$), the displacements at all nodes on the internal boundary are identical, again determining n of the integration constants, and the resulting n by n stiffness matrix includes only the degrees of freedom on the external boundary.

4. Side-face loads

When side-face loads are present, a general solution to the non-homogeneous differential equation (Eq. (27)) may be sought as a linear combination of the general solution of the homogeneous version and a particular solution of the same form as the term $\xi\{F_t(\xi)\}$. Since the general solution of the homogeneous equation is interpreted above as the combination of deformation modes, each of which closely satisfies internal equilibrium in the ξ direction, the additional particular solution can also be interpreted as a mode of deformation which almost satisfies internal equilibrium with the side-face loads. The modes representing the general solution of the homogeneous equation are referred to here as the 'homogeneous' modes, allowing differentiation between the mode types.

If the side-face loads can be represented as power functions of ξ such that

$$\{F_t(\xi)\} = \xi^t\{F_t\} \tag{46}$$

the side-face load mode displacements are of the form

$$\{u_t(\xi)\} = \xi^{t+1}\{\phi_t\} \tag{47}$$

Substitution of Eq. (47) into Eq. (27) yields

$$[(t+1)^2[E^0] + (t+1)[[E^1]^T - [E^1]] - [E^2]]\{\phi_t\} + \{F_t\} = \{0\} \tag{48}$$

The displacements at the nodal points on S for the side-face load mode can be obtained by rearrangement as

$$\{\phi_t\} = [(t+1)^2[E^0] + (t+1)[[E^1]^T - [E^1]] - [E^2]]^{-1}\{-F_t\} \tag{49}$$

and the corresponding displacement at the boundary nodes are

$$\{\phi_{ti}\} = \xi_i^{t+1}\{\phi_t\} \tag{50}$$

and

$$\{\phi_{te}\} = \xi_e^{t+1}\{\phi_t\} \tag{51}$$

The equivalent nodal boundary forces in equilibrium with these displacements by substitution of Eq. (47) into Eqs. (25) and (26) as

$$\{q_{ti}\} = -\xi_i^{t+1}[(t+1)[E^0] + [E^1]^{\mathrm{T}}]\{\phi_{ti}\} \tag{52}$$

and

$$\{q_{te}\} = \xi_e^{t+1}[(t+1)[E^0] + [E^1]^T]\{\phi_{te}\} \tag{53}$$

For a given set of integration constants, the displacements at the boundary nodes are

$$\begin{Bmatrix} \{u_h(\xi_i)\} \\ \{u_h(\xi_e)\} \end{Bmatrix} = \begin{Bmatrix} \{\phi_{ti}\} \\ \{\phi_{te}\} \end{Bmatrix} + [\Phi]\{c\} \tag{54}$$

The equivalent nodal boundary forces in equilibrium with this displacement field are

$$\begin{Bmatrix} \{P_i\} \\ \{P_e\} \end{Bmatrix} = \begin{Bmatrix} \{q_{ti}\} \\ \{q_{te}\} \end{Bmatrix} + [Q]\{c\} \tag{55}$$

Rearranging Eq. (54), the integration constants can be found in terms of the nodal displacements

$$\{c\} = [\Phi]^{-1}\left\{\begin{Bmatrix} \{u_h(\xi_i)\} \\ \{u_h(\xi_e)\} \end{Bmatrix} - \begin{Bmatrix} \{\phi_{ti}\} \\ \{\phi_{te}\} \end{Bmatrix}\right\} \tag{56}$$

Substituting this equation into Eq. (55) and rearranging, the equilibrium requirement is reduced to

$$[Q][\Phi]^{-1}\left\{\begin{Bmatrix} \{u_h(\xi_i)\} \\ \{u_h(\xi_e)\} \end{Bmatrix} - \begin{Bmatrix} \{\phi_{ti}\} \\ \{\phi_{te}\} \end{Bmatrix}\right\} = \begin{Bmatrix} \{P_i\} \\ \{P_e\} \end{Bmatrix} - \begin{Bmatrix} \{q_{ti}\} \\ \{q_{te}\} \end{Bmatrix} \tag{57}$$

or

$$[K]\begin{Bmatrix} \{u_h(\xi_i)\} \\ \{u_h(\xi_e)\} \end{Bmatrix} = \begin{Bmatrix} \{P_i\} \\ \{P_e\} \end{Bmatrix} - \begin{Bmatrix} \{q_{ti}\} \\ \{q_{te}\} \end{Bmatrix} + [K]\begin{Bmatrix} \{\phi_{ti}\} \\ \{\phi_{te}\} \end{Bmatrix} \tag{58}$$

where

$$[K] = [Q]\,[\Phi]^{-1} \tag{59}$$

as before. Boundary conditions place constraints on subsets of the displacements and nodal forces on the internal and external boundaries as before, and solution proceeds in the usual manner.

5. Discussion

Although the semi-analytical nature of scaled boundary finite element method endows it with significant advantages, including the ability to model points of stress singularity and discontinuity accurately at the scaling centre and the ability to analyse unbounded domains, a significant limitation is the requirement that the derivative of θ with respect to s remain positive over the defining curve S. A domain for which no single scaling centre exists which satisfies this requirement is shown in Fig. 4a, in which the curve S is taken as the exterior boundary while the

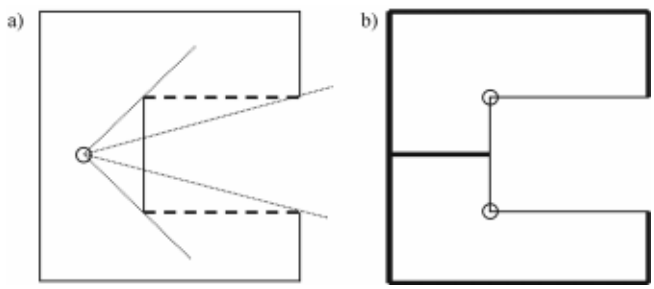

Fig. 4 A domain that must be sub-structured. a) Defining curve with sections over which $d\theta/ds$ is non-positive, b) Discretisation with two sub-domains, with heavy lines representing defining curves

interior boundary is at the scaling centre. Fortunately this limitation can be overcome easily by using a sub-structuring technique.

Since the scaled boundary finite-element method finds the stiffness of a domain relative to nodes located along its boundary, such domains can be assembled together as 'super-elements' before the nodal displacements are computed. This is illustrated in Fig. 4b. Once the boundary displacements have been found, internal displacements and stresses for each domain can be computed. Each domain has its own scaling centre and (possibly) two side-faces. The super-elements can only be connected along discretised boundaries, not along side-faces.

The analysis of domains with two similar boundaries, as described in this paper, may at first sight appear to have limited application (although Example 1 shows it can be used directly in some situations). However, the range of application is dramatically increased by using such domains as super-elements. The domains can then be used in combination with bounded domains containing the scaling centre, or domains modelled by alternative methods (such as the finite element method).

Perhaps the most significant application of the method is to provide transition super-elements between regions of coarse discretisation and regions of very fine discretisation. The boundaries of many structural mechanics problems contain 'sharp' corners. However, on close inspection these corners are actually curved or filleted. The detail of a corner dramatically effects the concentration of stress in the region. The length scale of the corner geometry is generally very much smaller than the length scale of the structure itself (for example a 5 mm radius on a 1 m square penetration through a wall). Should the standard finite element method be used to model such a problem, a very large number of elements is needed to provide the transition between the two geometric scales. Example 2 indicates how simply such problems can be handled using a domain with similar boundaries.

No special treatment is require to assemble transition super-elements (the stiffness matrix of which is determined by Eq. (42)) with traditional finite elements. Providing the shape functions used in the finite elements are of the same type and order as those used in the adjoining scaled boundary finite-elements, C^0 continuity of the displacement field will be preserved, and the model will be well behaved. Multiple transition super-elements with distinct scaling centres can be used in the same model, providing the super-elements are connected along discretised boundaries.

6. Examples

6.1 Example 1-compression of a thick-walled flattened tube

The structure in the first example contains two similar boundaries, and can consequently be solved using a single domain. The structure is a long thick-walled tube that lies horizontally on a flat rigid support. The tube is flattened top and bottom. The flattened bottom section is in contact with the support, while the flattened top section is subjected to a unit pressure loading. The cross-section of the tube is illustrated in Fig. 5a. The symmetry of the problem is taken into account, and only half of the problem modelled. Due to the length of the tube, plane strain conditions are assumed, and Poisson's ratio is taken as 0.25. The interface between the tube and the support is taken to be frictional with no slip occurring. The initial scaled boundary finite-element mesh is illustrated in Fig. 5b. To verify the accuracy and efficiency of the proposed approach, the problem is also analysed using the standard finite element method. The initial finite element mesh is shown in Fig. 5c.

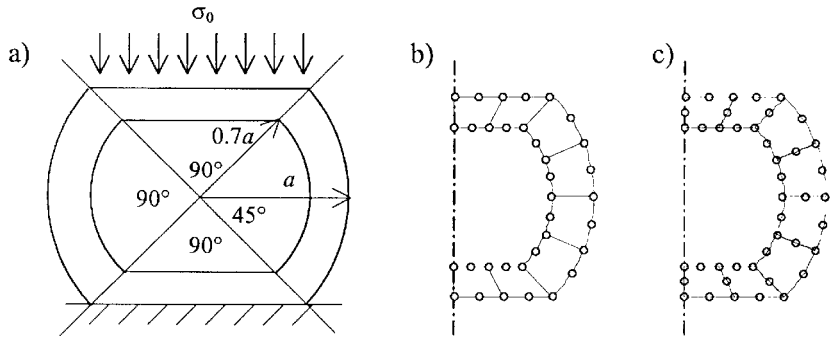

Fig. 5 Example 1-a) geometry and loading, b) initial scaled boundary finite-element mesh, c) initial finite element mesh

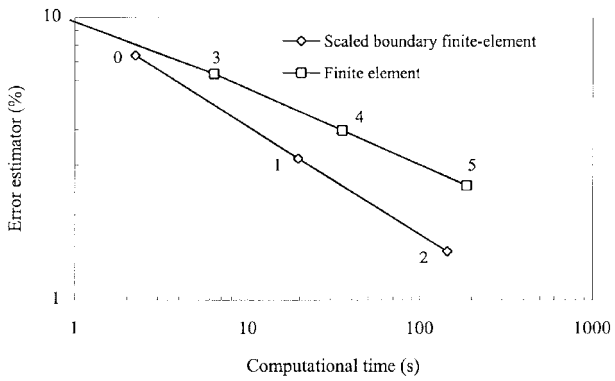

Fig. 6 Relationship between the error estimator and computational time for Example 1

The accuracy of the analysis results is determined using a recovery-based error estimator of the Zienkiewicz-Zhu type (1987). The computation of this error estimator for the scaled boundary finite element method is described by Deeks and Wolf (2002b). Extension to domains with similar boundaries is achieved by a simple modification of the integration bounds. Computational time is measured on a 450 MHz Pentium III PC using similar programs for both the scaled boundary finite-element method and the standard finite element method. The rate convergence of each method is evaluated by using a series of meshes of increasing fineness constructed by binary subdivision of the meshes shown in Fig. 5. The rate of convergence of the error estimator with mesh size and computational time is shown in Fig. 6. The numbers against the data points indicate the number of subdivisions of the initial mesh required to achieve the recorded level of accuracy. The efficiency of the scaled boundary finite-element method is seen to exceed that of the standard finite element method, and the computational savings at small error targets are seen to be considerable.

The vertical stresses computed with both the scaled boundary finite-element method and the finite element method are contoured in Fig. 7, normalised by the vertical stress on the top of the pipe, σ_0. Close agreement between the two is evident. The other stress components (which are not presented) show similar agreement. Overall this example demonstrates the accuracy and efficiency of the method presented in this paper for the analysis of domains with two similar boundaries.

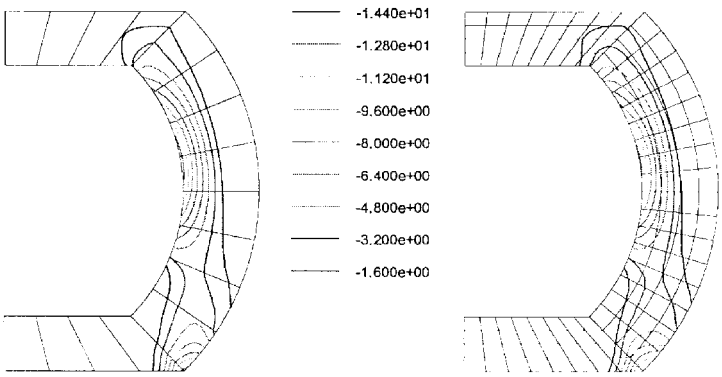

Fig. 7 Contours of vertical stress computed for Example 1 by the second mesh of the scaled boundary finite-element method (left) and the third mesh of the finite element method (right)

6.2 Example 2-plate containing a square hole with rounded corners under uniaxial tension

The final example illustrates perhaps the most effective use of the scaled boundary finite-element domains with similar boundaries. The problem is a square plate containing a square hole under uniaxial tension. If the corner of the hole is sharp, the stress at the corner is singular. However, in most situations the corner is actually rounded or filleted on a scale much smaller than the scale of the structure. Here the plate is taken to measure 4*a* by 4*a* and the hole is taken to measure 2*a* by 2*a*. The corners of the hole have a radius of *a*/75. The geometry of the problem is shown in Fig. 8. Due to symmetry only one quarter of the problem is modelled. The radius is not shown to scale. Poisson's ratio is taken as 0.25.

Since the boundary varies smoothly in the vicinity of the corner, the stress variation in this region will also be smooth, but will occur on a scale similar to the radius of the curve. Consequently the finite elements required to model this area accurately are very small. If the problem is modelled completely with finite elements, a very large number of elements is required to transition from the outer region (where the stress gradients are quite small) to the region near the corner. Here the

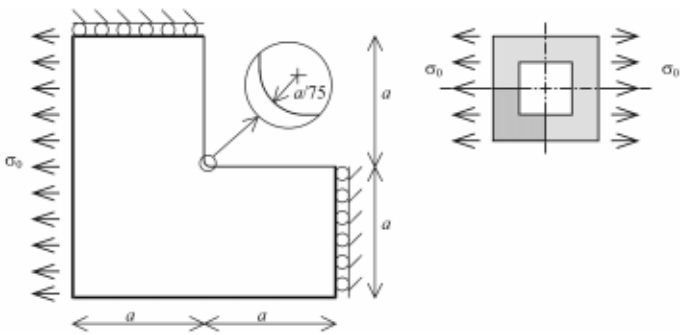

Fig. 8 Example 2-a square hole with rounded corners in a plate subjected to uniaxial tension

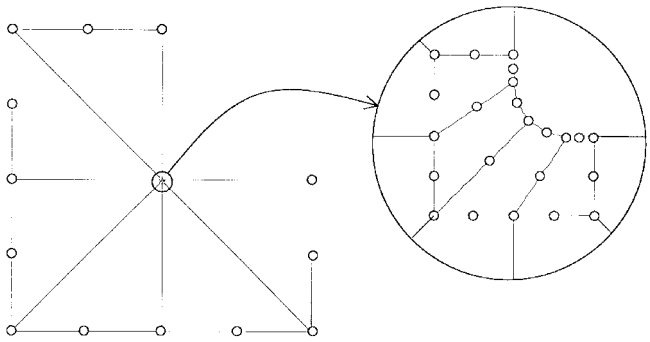

Fig. 9 Initial combined scaled boundary finite-element mesh/finite element mesh for Example 2

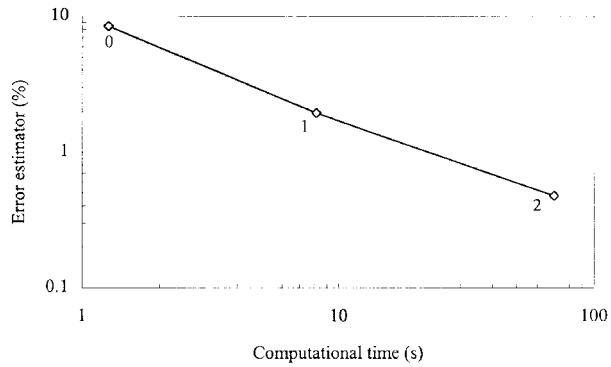

Fig. 10 Relationship between error estimator and computational time for Example 2

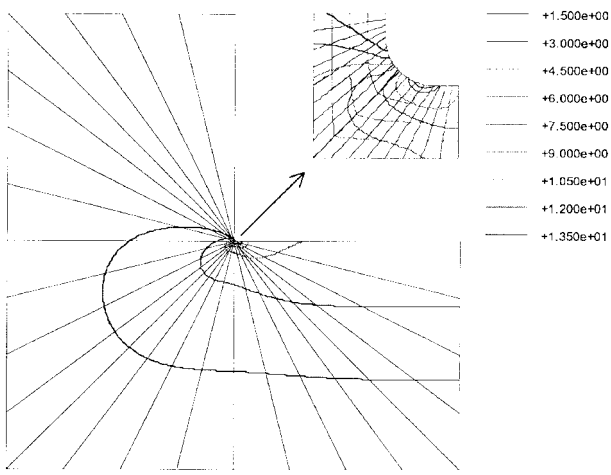

Fig. 11 Contours of horizontal stress for Example 2 in terms of σ_0 computed with the third mesh

scaled boundary finite-element domain with similar boundaries is used to provide that transition analytically. The region near the corner is modelled with finite elements. The initial combined scaled boundary finite-element mesh/finite element mesh is illustrated in Fig. 9. The radius and the finite elements are shown to scale in the diagram to the left, but cannot be distinguished clearly at this scale. The inset diagram magnifies the mesh present at the corner. Quadratic scaled boundary finite-elements with six boundary nodes (three on the interior boundary and three on the external boundary) are used away from the corner, while eight-noded quadratic isoparametric finite elements are used in the region near the corner.

The problem is analysed for the initial mesh and two finer meshes generated by binary subdivision of the initial mesh. The monotonic convergence of the error estimator with computational time is illustrated in Fig. 10, which indicates the procedure is well behaved.

The horizontal stresses computed by the third mesh are plotted in Fig. 11 in terms of σ_0. These stress contours are seen to pass smoothly between the regions modelled in different ways. Overall the procedure is seen to allow the stress concentrations near corners to be determined efficiently with few degrees of freedom.

7. Conclusions

This paper extends the semi-analytical scaled boundary finite-element method to the elastostatic analysis of domains containing two similar boundaries. The scaled boundary finite-element equation in displacement is not changed, but use is made of all the independent displacement 'modes' computed from the resulting quadratic eigenproblem. Depending on the side-face restraints up to two additional logarithmic modes may also be required. Unbounded domains may be considered as the special case where the external boundary is taken at infinity, and bounded domains containing the scaling centre as the special case where the internal boundary is taken at the scaling centre.

The equations are developed using a virtual work approach, and side-face loads are addressed. The solution process is described in full, and the role of sub-structuring in allowing efficient use of the technique is discussed.

Two examples are provided illustrating the use of the new technique to solve problems containing similar boundaries, and to provide a transition super-element between regions of vastly different scale. This last application is potentially the most useful ability of the method, as it allows stress concentrations at corners of extremely small radius to be computed efficiently. Results for the first example are compared with finite element solutions to establish the accuracy and efficiency of the technique. The new method is seen to work well and to increase the range of application of the scaled boundary finite-element method.

References

Banerjee, P.K. and Butterfield, R. (1981), *Boundary Element Methods in Engineering Science.* McGraw-Hill Book Co. (UK): London, New York.

Brebbia, C.A. and Walker, S. (1980), *Boundary Element Techniques in Engineering.* Newnes-Butterworths: London, Boston.

Cheung, M.S., Li. W. and Chidiac. S.E. (1996), *Finite Strip Analysis of Bridges*. E & FN Spon: London.

Cheung, Y.K. (1976), *Finite Strip Method in Structural Analysis*. Pergamon Press: Oxford, New York.
Deeks, A.J. and Wolf, J.P. (2002a), "A virtual work derivation of the scaled boundary finite-element method for elastostatics", *Comput. Mech.*
Deeks, A.J. and Wolf, J.P. (2002b), "Stress recovery and error estimation for the scaled boundary finite-element method", *Int. J. Numer. Meth. Eng.*
Deeks, A.J. and Wolf, J.P. (2002c), "Semi-analytical elastostatic analysis of unbounded two-dimensional domains", *Int. J. Numer. Anal. Meth. Geomechanics.*
Song, C.H. and Wolf, J.P. (1996), "Consistent infinitesimal finite-element cell method: three dimensional vector wave equation", *Int. J. Numer. Meth. Eng*, **39**, 2189-2208.
Song, C.H. and Wolf, J.P. (1997), "The scaled boundary finite-element method-alias consistent infinitesimal finite-element cell method-for elastodynamics", *Comp. Meth. Appl. Mech. Eng.*, **147**, 329-355.
Song, C.H. and Wolf, J.P. (1998), "The scaled boundary finite-element method: analytical solution in frequency domain", *Comp. Meth. Appl. Mech. Eng.*, **164**, 249-264.
Song, C.H. and Wolf, J.P. (1999), "Body loads in scaled boundary finite-element method", *Comp. Meth. Appl. Mech. Eng*., **180**, 117-135.
Szabó, B. and Babuška, I. (1991), *Finite Element Analysis*. J. Wiley: NewYork, Chichester, Brisbane.
Wolf, J.P. and Song, C.H. (1996), *Finite-Element Modelling of Unbounded Media*. John Wiley and Sons: Chichester.
Wolf, J.P. and Song, C.H. (2001), "The scaled boundary finite-element method-a fundamental-solution-less boundary-element method", *Comp. Meth. Appl. Mech. Eng.*, **190**, 5551-5568.
Zienkiewicz, O.C. and Taylor, R.L. (1989), *The Finite Element Method*. 4th ed. McGraw-Hill: London, New York.
Zienkiewicz, O.C. and Zhu, J.Z. (1987), "A simple error estimator and adaptive procedure for practical engineering analysis", *Int. J. Numer. Meth. Eng.*, **24**, 337-357.

Appendix A: Vector and matrix definitions for plane stress and strain

In the case of plane stress and plane strain, the displacement field has two components, displacement in the x-direction (u_x) and displacement in the y-direction (u_y).

$$\{u\} = \begin{Bmatrix} u_x \\ u_y \end{Bmatrix} \tag{A1}$$

Stress and strain have three independent components.

$$\{\sigma\} = \begin{Bmatrix} \sigma_x \\ \sigma_y \\ \tau_{xy} \end{Bmatrix} \tag{A2}$$

$$\{\varepsilon\} = \begin{Bmatrix} \varepsilon_x \\ \varepsilon_y \\ \gamma_{xy} \end{Bmatrix} \tag{A3}$$

The linear operator relating strain and displacement is

$$[L] = \begin{bmatrix} \frac{\partial}{\partial x} & 0 \\ 0 & \frac{\partial}{\partial y} \\ \frac{\partial}{\partial y} & \frac{\partial}{\partial x} \end{bmatrix} \tag{A4}$$

The elasticity matrix for plane stress is

$$[D] = \frac{E}{1-\nu^2}\begin{bmatrix} 1 & \nu & 0 \\ \nu & 1 & 0 \\ 0 & 0 & \frac{1-\nu}{2} \end{bmatrix} \tag{A5}$$

and for plane strain

$$[D] = \frac{E}{(1+\nu)(1-2\nu)}\begin{bmatrix} 1-\nu & \nu & 0 \\ \nu & 1-\nu & 0 \\ 0 & 0 & \frac{(1-2\nu)}{2} \end{bmatrix} \tag{A6}$$

where E and ν are Young's modulus and Poisson's ratio respectively.

Appendix B: Transformation to the scaled boundary coordinate system

The scaling equations relating the Cartesian coordinate system to the scaled boundary coordinate system are

$$x = x_0 + \xi\, x_s(s) \tag{B1a}$$

$$y = y_0 + \xi\, y_s(s) \tag{B1b}$$

Derivatives in the scaled boundary coordinate system can be related to derivatives in the Cartesian coordinate system using the Jacobian matrix.

$$\begin{Bmatrix} \frac{\partial}{\partial \xi} \\ \frac{\partial}{\partial s} \end{Bmatrix} = \begin{bmatrix} \frac{\partial x}{\partial \xi} & \frac{\partial y}{\partial \xi} \\ \frac{\partial x}{\partial s} & \frac{\partial y}{\partial s} \end{bmatrix} \begin{Bmatrix} \frac{\partial}{\partial x} \\ \frac{\partial}{\partial y} \end{Bmatrix} \tag{B2}$$

Taking derivatives of Eqs. (B1) with respect to ξ and s and rearranging

$$\begin{Bmatrix} \frac{\partial}{\partial \xi} \\ \frac{1}{\xi}\frac{\partial}{\partial s} \end{Bmatrix} = \begin{bmatrix} x_s(s) & y_s(s) \\ x_s(s),_s & y_s(s),_s \end{bmatrix} \begin{Bmatrix} \frac{\partial}{\partial x} \\ \frac{\partial}{\partial y} \end{Bmatrix} \tag{B3}$$

Inverting yields

$$\begin{Bmatrix} \frac{\partial}{\partial x} \\ \frac{\partial}{\partial y} \end{Bmatrix} = \frac{1}{|J(s)|}\begin{bmatrix} y_s(s),_s & -y_s(s) \\ -x_s(s),_s & x_s(s) \end{bmatrix} \begin{Bmatrix} \frac{\partial}{\partial \xi} \\ \frac{1}{\xi}\frac{\partial}{\partial s} \end{Bmatrix} \tag{B4}$$

where the Jacobian at the curve $S(\xi = 1)$ is

$$|J(s)| = x_s(s)\, y_s(s),_s - y_s(s)\, x_s(s),_s \tag{B5}$$

For plane stress and plane strain problems the incremental 'volume' is

$$dV = |J(s)|\, \xi\, d\xi\, ds \tag{B6}$$

If the linear operator is decomposed as

$$[L] = [L^1]\frac{\partial}{\partial x} + [L^2]\frac{\partial}{\partial y} \tag{B7}$$

using Eq. (B4) yields

$$\begin{aligned}[L] &= \frac{1}{|J(s)|}\left[[L^1]\left(y_s(s),_s\frac{\partial}{\partial \xi} - y_s(s)\frac{1}{\xi}\frac{\partial}{\partial s}\right) + [L^2]\left(-x_s(s),_s\frac{\partial}{\partial \xi} + x_s(s)\frac{1}{\xi}\frac{\partial}{\partial s}\right)\right] \\ &= [b^1(s)]\frac{\partial}{\partial \xi} + [b^2(s)]\frac{1}{\xi}\frac{\partial}{\partial s}\end{aligned} \tag{B8}$$

where

$$[b^1(s)] = \frac{1}{|J(s)|}[[L^1]y_s(s),_s - [L^2]x_s(s),_s] \tag{B9}$$

$$[b^2(s)] = \frac{1}{|J(s)|}[-[L^1]y_s(s) + [L^2]x_s(s)] \tag{B10}$$